Waves in Random and Complex Media

https://www.tandfonline.com/journals/twrm20

Accepted February 27th 2022

COMPUTATION OF BIO-NANO-CONVECTION POWER LAW SLIP FLOW FROM A NEEDLE WITH BLOWING EFFECTS IN A POROUS MEDIUM

J. Uddin[1,2*], N.A. Amirsom[1], **O. Anwar Bég[3]** & A. I. Ismail[1]

[1]School of Mathematics Sciences, Universiti Sains Malaysia, 11800, Penang, Malaysia.
[2]Prof. and Head, Department of Mathematics, American International University, Bangladesh, Kuril, Dhaka, 1229, Bangladesh.
[3]Professor and Director-Multi-physical Engineering Sciences Group (MPESG), Mechanical Engineering Department, SEE, Salford University, Manchester, M54WT, UK.
Email addresses: jashim_74@yahoo.com, ardiana5178@gmail.com, OA.Beg@salford.ac.uk, ahmad_izani@usm.my

Abstract

Transport phenomena with fluid flow, heat, mass, nanoparticle species and microorganism transfer external to a needle in a porous medium have many biomedical engineering applications (e. g. hypodermic needles used in hemotology). It is also used to design many biomedical engineering equipments and coating flows with bio-inspired nanomaterials. Coating flows featuring combinations of nanoparticles and motile micro-organisms also constitute an important application area. A mathematical model for convective external boundary layer flow of a power-law nanofluid containing gyrotactic micro-organisms past a needle immersed in a Darcy porous medium is developed. Multiple slips boundary conditions and Stefan blowing effects at the needle boundary are taken into account. The model features a reduced form of the conservation of mass, momentum, energy, nanoparticle species and motile micro-organism equations with appropriate coupled boundary conditions. The governing nonlinear partial differential equations (NPDEs) are converted to dimensionless form and appropriate invariant transformations are applied to obtain similarity ordinary differential equations (SODE). The transformed equations have been solved numerically using the in-built Matlab bvp4c function. The influence of the emerging parameters on the dimensionless velocity, temperature, nanoparticle concentration, motile micro-organism density functions, skin friction, heat, mass, and micro-organism transfers) are discussed in detail. It is found that velocity decreases whilst temperature, concentration, and density of motile micro-organism increase with an increase in blowing parameter for shear thinning (pseudoplastic), Newtonian, and shear thickening (dilatant) fluids. It is also found that skin friction, Nusselt number (dimensionless heat transfer rate), Sherwood number (dimensionless nanoparticle mass transfer rate) and motile micro-organism wall density gradient decrease with increasing blowing, Darcy, power law and needle size parameters. Comparison with the earlier published results is also included and an excellent agreement is obtained.

Keywords: *Biophysics, complex media, slip dynamics, non-Newtonian nanofluid, bioconvection.*

Nomenclature

A_1 constant $\left(m^2 / s\right)$

A_2 constant $\left(1 / m^{1+m}\right)$

$\tilde{b}$ chemotaxis constant (m)

C nanoparticle concentration (-)

C_p specific heat at constant pressure $\left(J / Kg\, K\right)$

C_w needle surface concentration (-)

C_∞ free stream concentration (-)

$C_{f\bar{x}}$ local skin friction coefficient $(-)$

D_B Brownian diffusion coefficient $\left(m^2 / s\right)$

D_m micro-organism diffusivity coefficient $\left(m^2 / s\right)$

D_N micro-organism diffusivity coefficient $\left(m^2 / s\right)$

D_T thermophoretic diffusion coefficient $\left(m^2 / s\right)$

Da Darcy number $(-)$

$D(\bar{x})$ thermal slip factor (m)

$E(\bar{x})$ mass slip factor (m)

$f(\eta)$ dimensionless stream function $(-)$

$F(\bar{x})$ micro-organism slip factor (m)

k permeability of the porous medium $\left(m^2\right)$

k_0 constant $\left(m^{1+m}\right)$

K consistency of the porous medium $\left(Pa\,s^{n}\right)$

Lb bioconvection Lewis number $(-)$

m power-law index for non-isothermal, non-iso-concentration (nanoparticle) and micro-organism non-iso-density conditions at the wall

n power law rheological index parameter $(-)$

$N_1(\bar{x})$ velocity slip factor $\left(sm^{-1}\right)$

Nb Brownian motion parameter $(-)$

$N_{n_{\bar{x}}}$ local density number of motile micro-organisms $(-)$

Nt thermophoresis parameter $(-)$

$N_{u_{\bar{x}}}$ local Nusselt number $(-)$

N number of motile micro-organisms $(-)$

N_w number of motile micro-organisms at wall (wedge face) $(-)$

N_∞ ambient number of motile micro-organisms $(-)$

Pe Péclet number $(-)$

Pr Prandtl number $(-)$

$Re_{\bar{x}}$ local Reynolds number $(-)$

Sc Schmidt number $(-)$

$Sh_{\bar{x}}$ local Sherwood number $(-)$

T nanofluid temperature (K)

T_w dimensional surface temperature at the wall (K)

T_∞ dimensional ambient temperature (K)

$\bar{u}, \bar{v}$ dimensional velocity components along the $\bar{x}-$ and $\bar{r}-$axes (m/s)

$\bar{u}_e$ external velocity (m/s)

u_1 constant (m^{1-m}/s)

W_c maximum cell swimming speed (m/s)

$\bar{x}, \bar{r}$ coordinates along and normal to the needle (m)

Greek symbols

α effective thermal diffusivity (m^2/s)

η independent similarity variable $(-)$

μ dynamic viscosity of the fluid (kg/ms)

δ_C mass slip parameter $(-)$

δ_N microorganism slip parameter $(-)$

δ_T thermal slip parameter $(-)$

δ_u velocity slip parameter $(-)$

υ kinematic viscosity of the fluid (m^2/s)

ρ fluid density (kg/m^3)

$(\rho c)_f$ heat capacitance of the base fluid (J/m^3K)

$(\rho c)_p$ heat capacitance of the nanoparticles (J/m^3K)

τ ratio of the effective heat capacity of the nanoparticle to the fluid heat capacity $(-)$

θ dimensionless temperature $(-)$

ϕ dimensionless concentration $(-)$

χ dimensionless number density of motile microorganisms $(-)$

ψ dimensionless stream function $\left(m^3 / s\right)$

Subscripts

$( )'$ differentiation with respect to η

1.Introduction

Transport phenomena with fluid flow, heat, nanoparticle species and microorganism transfer external to axisymmetric bodies (e.g. needles) in a porous medium is a dynamic research area due to its relevance to a number of areas of engineering and technology. For example, in biomedical engineering such flows may arise in hypodermic needles used in hemotology. Coating flows featuring combinations of nanoparticles and motile micro-organisms also constitute an important application area [1]. According to published books [2-3] and published papers [4], both natural and artificial porous media arise in biological and biomedical applications, namely magnetic resonance imaging (MRI), drug delivery (pharmacodynamics) and biotechnological manufacturing systems (linctuses, hydrogels, hyaluronic-based lubricants, antiseptic lotions etc). Porous media can be used to enhance heat transfer rates. Examples include metallic foams, fibrous media, tissue, cartilage and organs. Nanomedicine has emerged as a vibrant new field in which both nanomaterials and nanoscale design are increasingly used to achieve improved treatments [5-7]. In parallel with these clinical investigations, recently, a number of analytical and computational fluid dynamics studies of external flow with heat, mass and microorganisms transfer from needle-like geometries, has received significant attention due to rising applications [8-10]. Ishak *et al*. [11] simulated the convective flow due to a moving needle. Trimbitas *et al*. [12] computed the nanofluid flow over a thin needle using the bvp4c function in combination with chebfun package

from Matlab. Hayat *et al.* [13] studied water-based nanofluid flow taking into account variable heat flux using a numerical shooting method. Radiative free convective heat and mass transfer in a porous medium was studied by Bano & Singh [14] using combined integral and shooting methods. Entropy generation and radiation effects in external boundary layer flow from a needle were examined by Afridi & Qasim [15] using the MATLAB in-built solver bvp4c and shooting technique. Krishna *et al.* [16] studied MHD Sakiadis and Blasius flows of nanofluids from a needle. Sulochana *et al. [17]* extended the work of Krishna *et al.* [16] to consider Ohmic dissipation in magnetic nanofluid flow from a needle. In another paper, Afridi *et al.* [18] conducted a second law thermodynamic analysis of radiative dissipative flow and heat transfer for water-based nanofluids containing carbon nanotubes. Salleh *et al.* [19] studied numerically the nanofluid flow from a moving needle in a nanofluid numerically also considering stability of the solution. Souayeh *et al.* [20] utilized a Runge-Kutta method with shooting technique to investigate the effect of non-linear radiative heat flux on viscoplastic nanofluid flow from a thin needle. Further details concerning the many types and synthesis methods for nanofluids (nanoparticles, nanotubes, nanowires etc suspended in different base fluids) are documented in monographs [21-22] and in a variety of articles [23-25].

In recent years engineers have increasingly explored biological mechanisms for improving technical designs. Many exciting areas have emerged in this regard including biomimetic boundaries, self-healing, adaptive materials and also exotic propulsion mechanisms. An attractive propulsion mechanism used by micro-organisms is bioconvection which refers to the macroscopic swimming of micro-organisms resulting from a transition in the presence of a density gradient**.** Micro-organisms play a vital role in numerous ecological, biological, medical and engineering phenomena [26-27]. Microorganisms are also advantageous in food production, in the treatment of wastewater, biofuels, chemical bioreactors and enzymes. Bioconvecting micro-

organisms respond to a number of different stimuli (e.g. light, gravity, chemical or magnetic fields, oxygen). This mechanism is known as *taxis* (e.g. gravitaxis, gyrotaxis, geotaxis, phototaxis, oxytaxis, chemotaxis etc). In the case of *gravitaxis*, microorganisms swim in the reverse direction of gravity whilst in *gyrotaxis*, micro-organism swimming is controlled by the torque produced due to gravity force and viscous forces. In the case of phototaxis, micro-organisms swim in the direction of, or away from light [28]. Both experimental and theoretical studies have revealed that the addition of micro-organisms to nanofluids yields superior thermal performances and also beneficial "green" characteristics in for example next generation biofuels. Nanofluid bioconvection boundary layer flows are especially important in the vicinity of the internal walls of bio-engineered micro/nanodevices. The nano-bioconvection transport phenomena are governed by the balance of mass, momentum, energy and micro-organism species [29-30] along with relevant physically realistic boundary conditions (for example slip and blowing). Many engineering applications of nanofluid bioconvection including rotating nano-doped bioreactors (Von Karman swirling flows) were recently discussed by Bég et al. [31]. Currently, transport problems due to combined nanofluid bioconvection flows external to various geometries (disk, cone, flat plate, wedge, channel, needle) have received substantial attention among applied mathematicians and engineering scientists. Water-based nano-bioconvection boundary layer flow from a wavy surface was addressed by Siddiqa *et al*. [32] using a finite difference based numerical method. Ferdows *et al.* [33] used CODEBLOCKS numerical routines to compute the stagnation bioconvection nanofluid flow from stretching and shrinking sheets with applications in coatings. Bég *et al.* [34], studied the bioconvection nanofluid flow from a rotating porous disk to a Darcian porous medium with anisotropic slip effects. Bioconvection due to gravitactic microorganisms was studied by Mil-Martínez et al. [27] using numerical methods. MHD bioconvection of Williamson nanofluid was studied numerically using Matlab bvp4c technique by Zaman and Gul [35].

Non-Newtonian fluids are significant in numerous industries such as polymer coatings, petro-chemical processing, bio-chemical synthesis etc. Various non-Newtonian models have been studied by the researchers for thermosolutal transport phenomena external to various geometries taking into account various thermophysical effects (e.g. magnetic fields, wavy walls, species diffusion, Brinkman vorticity diffusion, Marangoni convection, electrophoresis, thermal stratification etc.). Various mathematical modelling studies of non-Newtonian transport in porous media can be found in the books [36]. Khan *et al.* [37] studied power-law nanofluid bioconvection boundary layer flow from a vertical plate. Kefayati [38] studied heat transfer and entropy generation in pseudoplastic nanofluids in a porous medium cavity with a finite difference lattice Boltzmann method (FDLBM) and Darcy model**.** Huang [39] studied free convective flow in rheological power-law nanofluids along a permeable plate with thermal radiation and the Keller box finite difference method. Waqas *et al.* [40] studied numerical computations of a viscoelastic Reiner-Rivlin second grade nanofluid doped with gyrotactic micro-organism over a deformable sheet. Very recently, Amirsom et al. [41] studied magnetohydrodynamic bio-nano-convective non-Newtonian flow along a needle with Stefan blowing. Further studies of non-Newtonian transport with and without bioconvection in porous media include Roy *et al. [42]* (on Taylor dispersion in power-law blood flow through Darcy-Forchheimer porous biomaterials) and Umavathi and Bég [43] on thermosolutal hydrodynamic stability of polar (couple stress) nanofluid saturated porous media. Some other analytical and numerical approaches relevant to simulation of nanofluid flow doped with propelling micro-organisms include Rehman et al. [44], Rizwana et al. [45], Ahmad et al. [46], Hussain et al. [47]. Hossen et al, [48] (on the modified double sub-equation method for finding complexiton solutions to the (1+ 1) dimensional nonlinear evolution equations which may benefit deeper simulations of wave structures and evolution in propulsion of bacteria) and Roshid et al. [49] (on multi-soliton fusion phenomenon of Burgers equation and fission, fusion

phenomenon of Sharma–Tasso–Olver equation, which may also be relevant to analyzing propulsion waves generated by micro-organisms).

A careful examination of the literature has highlighted that bioconvection in external coating boundary layer flow of a power-law nanofluid (pseudoplastic/dilatant) over a thin fixed impermeable needle embedded in a Darcy porous medium, taking into account *multiple slips and Stefan blowing*, has not been reported in the literature. This is the focus of the present paper which significantly extends the earlier work of Amirsom *et al*. [41] for a Darcian porous medium saturated with both nanofluid and gyrotactic microorganisms and incorporates *multiple slip effects* (which are practicable in real systems). Extensive new results are also presented which provide a deeper appreciation of the mechanisms of transport within the bio-nano-boundary layer flow regime. The results reported are relevant to the improved design of biomedical needles and also coating applications in medical nano-systems. Comprehensive visualization of thermal, species (nanoparticles, micro-organisms) and flow characteristics are included, and the simulations furthermore provide a useful benchmark for more refined biomedical coating designs.

2. Rheological Bioconvective Nanofluid Multiple Slip Transport Model

The nanofluid bioconvection transport equations associated with the fluid flow, heat, nanoparticle species and microorganism species transfer are derived from earlier monographs and works [50]. Steady axisymmetric forced bioconvection power-law nanofluid flow (containing gyrotactic micro-organisms) in external boundary layer transport from a solid needle embedded in Darcy porous medium is considered. **Figure 1** displays the geometry of the problem under consideration. The radius of the slender paraboloid (e.g. hypodermic micro-needle) is designated by $\bar{r} = R(\bar{x})$. Here $\bar{x}$ and $\bar{r}$ are the axial and radial coordinates; the $\bar{x}$ -axis is measured from the leading edge of the needle. The nanoparticles added to the base fluid (water) are assumed dilute and do not alter the swimming direction or velocity of the micro-organisms. Stefan blowing on the wall is

incorporated. It is assumed that the porous medium and convective flow are isotropic and in thermal equilibrium. Thermophysical properties are assumed to be constant. The surrounding fluid is assumed to be maintained at a constant temperature T_∞ and concentration C_∞, while the body surface is prescribed variable temperature $T_w(\bar{x})$, nanoparticle concentration $C_w(\bar{x})$ and motile microorganism density number, $N_w(\bar{x})$. A variable potential flow velocity of the form $\overline{u_e} = u_1 \bar{x}^m$, is considered where u_1, m are dimensional constants. Using an order of magnitude analysis. the governing balance equations in cylindrical coordinates are obtained by extending the earlier model of Amirsom *et al.* [41] and take the form:

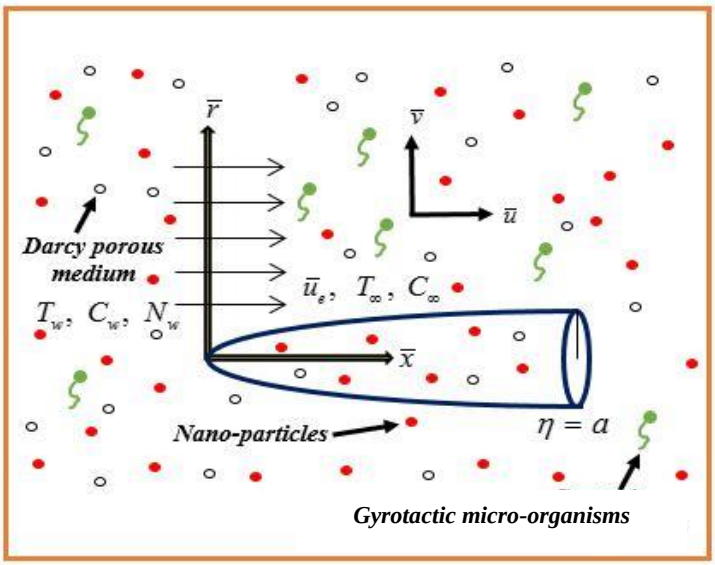

Figure 1 Geometry and coordinate system

$$\frac{\partial}{\partial \bar{x}}\left(\bar{r}\bar{u}\right)+\frac{\partial}{\partial \bar{r}}\left(\bar{r}\bar{v}\right)=0, \tag{1}$$

$$\bar{u}\frac{\partial \bar{u}}{\partial \bar{x}}+\bar{v}\frac{\partial \bar{u}}{\partial \bar{r}}=\overline{u_e}\frac{d\overline{u_e}}{d\bar{x}}+\frac{1}{\rho \bar{r}}\frac{\partial}{\partial \bar{r}}\left[\bar{r}\,\tau_{\bar{r}\bar{x}}\right]-\frac{\nu}{k(x)}\left(\bar{u}-\overline{u_e}\right), \tag{2}$$

$$\bar{u}\frac{\partial T}{\partial \bar{x}}+\bar{v}\frac{\partial T}{\partial \bar{r}}=\frac{\alpha}{\bar{r}}\frac{\partial}{\partial \bar{r}}\left(\bar{r}\frac{\partial T}{\partial \bar{r}}\right)+\tau D_B\frac{\partial T}{\partial \bar{r}}\frac{\partial C}{\partial \bar{r}}+\tau\frac{D_T}{T_\infty}\left(\frac{\partial T}{\partial \bar{r}}\right)^2, \tag{3}$$

$$\bar{u}\frac{\partial C}{\partial \bar{x}}+\bar{v}\frac{\partial C}{\partial \bar{r}}=\frac{D_B}{\bar{r}}\frac{\partial}{\partial \bar{r}}\left(\bar{r}\frac{\partial C}{\partial \bar{r}}\right)+\frac{D_T}{T_\infty}\frac{1}{\bar{r}}\frac{\partial}{\partial \bar{r}}\left(\bar{r}\frac{\partial T}{\partial \bar{r}}\right), \tag{4}$$

$$\bar{u}\frac{\partial N}{\partial \bar{x}}+\bar{v}\frac{\partial N}{\partial \bar{r}}+\frac{\tilde{b}W_c}{\left(C_w-C_\infty\right)}\left[\frac{\partial}{\partial \bar{r}}\left(N\frac{\partial C}{\partial \bar{r}}\right)\right]=\frac{D_N}{\bar{r}}\frac{\partial}{\partial \bar{r}}\left(\bar{r}\frac{\partial N}{\partial \bar{r}}\right). \tag{5}$$

Here $\tau_{\bar{r}\,\bar{x}}=K\left(\partial\bar{u}/\partial\bar{r}\right)^n$, $k\left(\bar{x}\right)=k_0/\left(\bar{x}\right)^{m-1}$, where *K* represents the rheological consistency index, *k* is the permeability of the porous medium, k_0 is a dimensional constant, *m* signifies an index representing non-isothermal, non-iso-concentration and microorganism non-iso-density conditions at the wall and *n* is the flow behaviour index of the power-law fluids. The model represents shear-thinning (pseudoplastic) fluids for *n < 1 and* shear-thickening (dilatant) fluids for *n > 1*. The traditional Newtonian fluid model is recovered for *n=1*. The relevant wall and free stream flow boundary conditions [51] are:

$$\begin{aligned}&\bar{r}=r(\bar{x}):\ \bar{u}=N_1(\bar{x})\nu\left(\partial\bar{u}/\partial\bar{r}\right),\quad \bar{v}=-(D_B/(1-C_w))\left(\partial C/\partial\bar{r}\right),\\&T=T_w\left(\bar{x}\right)+D(\bar{x})\left(\partial T/\partial\bar{r}\right),\quad C=C_w\left(\bar{x}\right)+E(\bar{x})\left(\partial C/\partial\bar{r}\right),\\&N=N_w\left(\bar{x}\right)+F(\bar{x})\left(\partial N/\partial\bar{r}\right)\end{aligned} \tag{6}$$

$$\bar{r}\to+\infty:\ \bar{u}=\overline{u_e},\quad T\to T_\infty,\quad C\to C_\infty,\quad N\to 0. \tag{7}$$

The following notation applies: ($\bar{u}$, $\bar{v}$): velocity components along the axes, ($\bar{x},\bar{r}$) : axial and radial coordinates, ρ : fluid density, $\tilde{b}$: chemotaxis constant, W_c : maximum cell swimming speed of microorganisms, $\left(D_B,D_T,D_N\right)$: Brownian, thermophoretic, and micro-organisms diffusion coefficients, $k(x)$: permeability of the porous medium, α : thermal diffusivity, $\left(N_1,D,E,F\right)$: velocity, thermal, mass, and microorganism slip factors prescribed at the needle surface.

Following Chen and Kearns [52], we adopt the following set of similarity transformations

$$\begin{aligned}&\eta=A_2\left(\bar{x}\right)^{m-1}r^2,\ \psi=A_1\bar{x}f\left(\eta\right),\ \theta\left(\eta\right)=(T-T_\infty)/(T_w-T_\infty),\\&\phi\left(\eta\right)=(C-C_\infty)/(C_w-C_\infty),\ \chi\left(\eta\right)=N/N_w.\end{aligned} \tag{8}$$

Here

$$A_1 = \left(K/\rho\right)^{2/(n+1)} u_1^{3(n-1)/(n+1)}, \quad A_2 = \left((\rho/K)u_1^{2-n}\right)^{2/(n+1)}, \quad T_w = T_\infty + T_0 \bar{x}^s,$$
$$C_w = C_\infty + C_0 \bar{x}^s, \; N_w = N_0 \bar{x}^s \tag{9}$$

Selecting an appropriate stream function, ψ defined by

$$\bar{u} = (1/\bar{r})(\partial\psi/\partial\bar{r}) \text{ and } \bar{v} = -(1/\bar{r})(\partial\psi/\partial\bar{x}). \tag{10}$$

The continuity equation (1) is thereby satisfied. By setting $\eta = a$, in the first equation of (8), where *a* is *numerically small for a thin needle*, a surface of revolution is represented which refers to the wall of the needle and using (8), Eqns. (2)-(7) are transformed into the following coupled, nonlinear similarity ordinary differential equations (SODEs)

$$2n(4)^n \eta^{(n+1)/2} \left(f''\right)^{n-1} f''' + \left(4\right)^n \left(n+1\right)\eta^{(n-1)/2}\left(f''\right)^n$$
$$+ 4ff'' - 4m\left(f'\right)^2 + m - (1/Da)\left(2f'-1\right) = 0, \tag{11}$$

$$2\eta\theta'' + 2\theta' + \Pr\left(f\theta' - sf'\theta\right) + Nb\theta'\phi' + Nt\theta'^2 = 0, \tag{12}$$

$$2\eta\phi'' + 2\phi' + Sc\left(f\phi' - sf'\phi\right) + (Nb/Nt)\left(2\eta\theta'' + 2\theta'\right) = 0, \tag{13}$$

$$2\eta\chi'' + 2\chi' + Lb\left(f\chi' - sf'\chi\right) - Pe\left(2\eta\chi\phi'' + 2\chi\phi' + 2\eta\phi'\chi'\right) = 0. \tag{14}$$

The associated boundary conditions emerge as:

$$f'(a) = 2\delta_u a^{1/2} f''(a), \quad f(a) = (2a\, fw/Sc)\,\phi'(a) - 2a^{3/2}(m-1)\delta_u f''(a),$$
$$\theta(a) = 1 + 2\delta_T a^{1/2}\theta'(a), \quad \phi(a) = 1 + 2a^{1/2}\delta_C\phi'(a), \quad \chi(a) = 1 + a^{1/2}\delta_N\chi'(a), \tag{15}$$

$$f'(+\infty) \to 1/2, \quad \theta(+\infty) \to 0, \quad \phi(+\infty) \to 0, \quad \chi(+\infty) \to 0 \tag{16}$$

The dimensionless parameters featured in Eqns. (11)-(16) are defined as follows:

$\Pr = A_1/\alpha$ (generalized Prandtl number), $Nb = \tau D_B\left(C_w - C_\infty\right)/\alpha$ (Brownian motion),

$Nt = \tau D_T\left(T_w - T_\infty\right)/\alpha T_\infty$ (thermophoresis), $Sc = A_1/D_B$ (Schmidt number),

$Da = \rho A_1 A_2/k_0$ (Darcy number), $Lb = A_1/D_m$ (bioconvection Lewis number),

$Pe = \tilde{b}W_c/D_m$ (Péclet number), $\delta_u = N_1(\bar{x})A_2^{1/2}\left(\bar{x}\right)^{(m-1)/2}$ (velocity slip),

$\delta_T = D(\bar{x})A_2^{1/2}\left(\bar{x}\right)^{(m-1)/2}$ (thermal slip), $\delta_C = E(\bar{x})A_2^{1/2}\left(\bar{x}\right)^{(m-1)/2}$ (mass slip),

$\delta_N = F(x)A_2^{1/2}x^{(m-1)/2}$ (microorganism slip), $fw = C_w/(1-C_w)$ (blowing).

For true similarity solutions velocity slip factor $N_1(\bar{x})$, thermal slip factor $D(\bar{x})$, mass slip factor $E(\bar{x})$, and microorganism slip factors $F(\bar{x})$ are proportional to $\left(\bar{x}\right)^{(1-m)/2}$.

It is important to note that $fw > 0$ signifies mass blowing (i.e. fluid moves out from the needle to the potential flow) whilst $fw < 0$ denotes mass suction (i.e. fluid moves into the needle from the potential flow). Also it is emphasized that in the *absence of Stefan blowing, nanofluid and bioconvection effects*, with no slip boundary conditions and absence of a porous medium $\left(Da \to \infty\right)$, the present model reduces to the non-isothermal power-law needle forced convection boundary layer flow model studied earlier by Chen & Kearns [52]). This earlier study is therefore employed as a benchmark for validating the new model. Of interest in biomedical coating design are the surface gradients of the variables (velocity, temperature, nanoparticle concentration and motile microorganism density number). These are known as the *local skin friction* $C_{f_{\bar{x}}}$, *Nusselt number* $Nu_{\bar{x}}$, *Sherwood number* $Sh_{\bar{x}}$, *and the gradient of density number of motile microorganisms* $Nn_{\bar{x}}$, respectively, and are defined as follows:

$$\begin{aligned} Cf_{\bar{x}} &= (K/(1/2)\rho\overline{u_e}^2)\left(\partial\bar{u}/\partial\bar{r}\right)^n_{\eta=a},\ Nu_{\bar{x}} = -\left(\bar{x}/(T_w - T_\infty)\right)\left(\partial\overline{T}/\partial\bar{r}\right)_{\eta=a}, \\ Sh_{\bar{x}} &= -(\bar{x}/D_B(C_w - C_\infty))\left(\partial\overline{C}/\partial\bar{r}\right)_{\eta=a},\ Nn_{\bar{x}} = (\bar{x}/D_N\, N_w)\left(\partial N/\partial\bar{r}\right)_{\eta=a}. \end{aligned} \tag{17}$$

Substituting Eqn. (8) into Eqn. (17) yields:

$$\begin{aligned} &Cf_{\bar{x}}\,\mathrm{Re}_{\bar{x}}^{1/(n+1)} = 2\left(4\right)^n a^{(n/2)}\left[\,f''\left(a\right)\right]^n, \quad \mathrm{Re}_{\bar{x}}^{-1/(n+1)}\,Nu_{\bar{x}} = -2a^{(1/2)}\theta'\left(a\right), \\ &\mathrm{Re}_{\bar{x}}^{-1(n+1)}\,Sh_{\bar{x}} = -2a^{(1/2)}\phi'\left(a\right), \quad \mathrm{Re}_{\bar{x}}^{-1/(n+1)}\,Nn_{\bar{x}} = -2a^{(1/2)}\chi'\left(a\right). \end{aligned} \tag{18}$$

Here $\mathrm{Re} = \rho u_1^{2-n}\bar{x}^n / K$ is the generalized Reynolds number and the primes denote differentiation with respect to η.

3. Numerical Solution and Validation

Numerical solutions of the transformed non-dimensional similarity ordinary differential equations (SODEs) i.e. (11) - (14) subject to the dimensionless imposed boundary conditions (15) - (16) are achieved utilizing MATLAB symbolic software with the inbuilt bvp4c function. This routine uses a finite difference coding that implements the three-stage Lobatto IIIa formula and produces continuous solutions within the boundary values with *fourth order accuracy* [53]. Several stages are inherent to using this algorithm. Firstly, one converts the higher order SODEs to a system of first order ODEs. Hence introducing the following variables:

$$\begin{aligned} &z_1 = f,\ z_2 = f',\ z_3 = f'', \\ &z_4 = \theta,\ z_5 = \theta' \\ &z_6 = \phi,\ z_7 = \phi', \\ &z_8 = \chi,\ z_9 = \chi'. \end{aligned} \tag{19}$$

Substituting Eqn. (19) into the SODE equations (11) - (14), we have the following system of first order ODEs:

$$\begin{pmatrix} f' \\ \theta' \\ \phi' \\ \chi' \\ z_3' \\ z_5' \\ z_7' \\ z_9' \end{pmatrix} = \begin{pmatrix} z_2 \\ z_5 \\ z_7 \\ z_9 \\ ((1/(2n4^n \eta^{(n+1)/2} z_3^{(n-1)})(-4^n(n+1)\eta^{(n-1)/2} z_3^n \\ -4z_1 z_3 + 4m z_2^2 - m + (1/Da)(2z_2 - 1)) \\ (1/2\eta)(-2z_5 - Pr(z_1 z_5 - s z_2 z_4) - Nb z_5 z_7 - Nt(z_5)^2) \\ (1/2\eta)(-2z_7 - Sc(z_1 z_7 - s z_2 z_6 - (Nb/Nt)(2\eta z_5' + 2z_5) \\ (1/2\eta)(-2z_9 - Lb z_1 z_9 - s z_2 z_8 + Pe(2\eta z_8 z_7' + 2z_7 z_8 + 2\eta z_7 z_9) \end{pmatrix} \tag{20}$$

The boundary conditions are now transformed to:

$$\left.\begin{aligned} &z_1(a) = (2af_w / Sc) z_7(a) - 2a^{3/2}(m-1)\delta_u z_3(a) \\ &z_2(a) = 2\delta_u a^{1/2} z_3(a) \\ &z_4(a) = 1 + 2\delta_T a^{1/2} z_5(a) \\ &z_6(a) = 1 + 2\delta_C a^{1/2} z_7(a) \\ &z_8(a) = 1 + 2\delta_N a^{1/2} z_9(a) \end{aligned}\right\} \tag{21}$$

In addition to the above boundary conditions, we have the following boundary conditions

$$\left.\begin{aligned} z_2(\infty)&=0.5 \\ z_4(\infty)&=0 \\ z_6(\infty)&=0 \\ z_8(\infty)&=0 \end{aligned}\right\} \tag{22}$$

The system of equations in (20) and boundary conditions in (21) and (22), have been solved using the MATLAB built function bvp4c.

Table 1 Values of heat transfer rates, $-\theta'(a)$ for surface temperature needles with $m = 1/3$

			Chen and Kearns [52]	Present Study (BVP4C)	Chen and Kearns [52]	Present Study (BVP4C)
n	s	Pr	$a = 0.01$	$a = 0.01$	$a = 0.1$	$a = 0.1$
0.5	0	0.733	17.0970	17.29390	2.6002	2.72503
		10	27.0610	27.43376	4.6879	4.68500
		100	45.0799	45.34437	8.6850	8.70852
		500	68.1350	68.82254	13.9700	14.01457
	1	0.733	20.0545	20.03143	3.1956	3.21639
		10	33.2316	33.05056	6.0189	6.01861
		100	57.5813	57.45699	11.4878	11.50361
		500	89.0979	89.42190	18.7008	18.73861
1	0	0.733	16.6200	16.69841	2.5084	2.50263
		10	24.8580	24.81458	4.2530	4.25196
		100	38.6160	38.6160	7.4256	7.42941
		500	55.4975	55.47167	11.5680	11.56892
	1	0.733	19.1577	19.16962	3.0221	3.02241
		10	29.6904	29.66865	5.3314	5.31752
		100	47.9085	47.89558	9.6461	9.64382
		500	70.7333	70.76323	15.2809	15.27177
1.5	0	0.733	16.3230	16.47394	2.4428	2.55598
		10	23.9770	23.89358	4.1088	4.10174
		100	36.1600	36.14587	7.0072	7.01136
		500	50.8700	51.04056	10.7700	10.76123
	1	0.733	18.7962	18.74672	2.9656	2.96636
		10	28.3043	28.22382	5.1012	5.09630
		100	44.3077	44.33524	9.0331	9.04957
		500	64.0730	64.30963	14.1469	14.12595

In order to validate our simulated results, comparison has been made with previously published data from the literature [52] and for the skin friction in Table 1, and for heat transfer rate in Table 2, and favourable agreement is achieved for both cases. Confidence in the MATLAB solutions is therefore established.

Table 2 Values of friction, $f''(a)$ for surface temperature needles with $m = 1/3$

	Chen and Kearns [52]	Present Study (BVP4C)	Chen and Kearns [52]	Present Study (BVP4C)
n	$a = 0.01$	$a = 0.01$	$a = 0.1$	$a = 0.1$
0.5	28.3061	28.21138	3.4569	3.47866
1	9.9479	9.92894	1.6155	1.61625
1.5	6.1786	6.17781	1.1959	1.19272

4. MATLAB Results and Discussion

A detailed parametric study of the impact of key parameters on transport characteristics is conducted and the results are presented graphically in **Figs. 2-15**. Appropriate data is selected to be representative of actual bioconvection nanofluid coating flows in hypodermic needle applications- see Cevc and Vierl [5] and Bég [31].

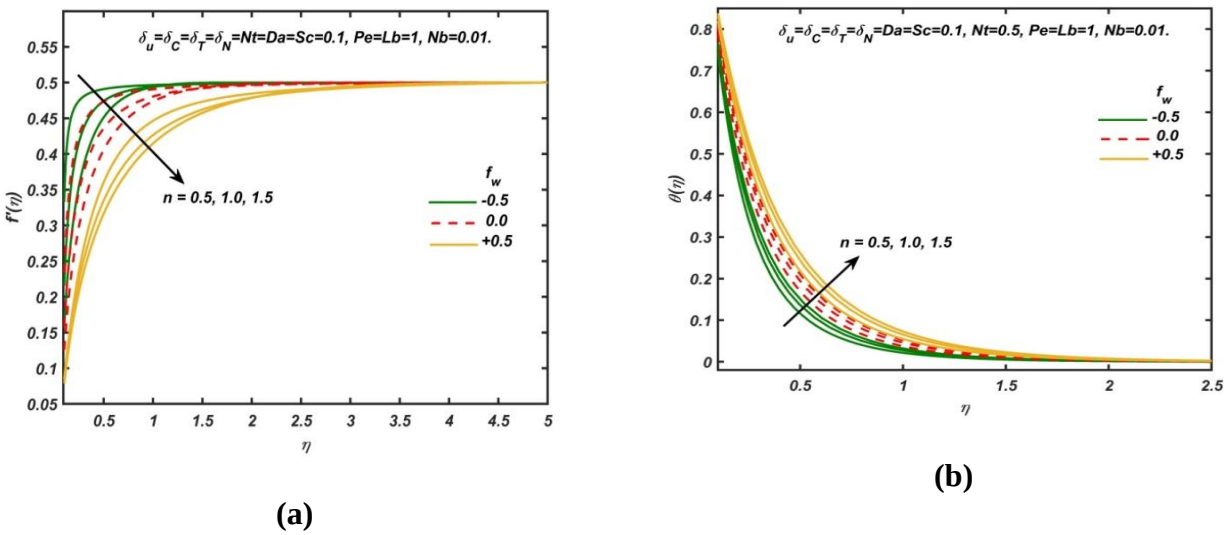

(a) **(b)**

Figure 2 Effect of blowing and power law rheological index parameters on (a) the dimensionless velocity and (b) the temperature.

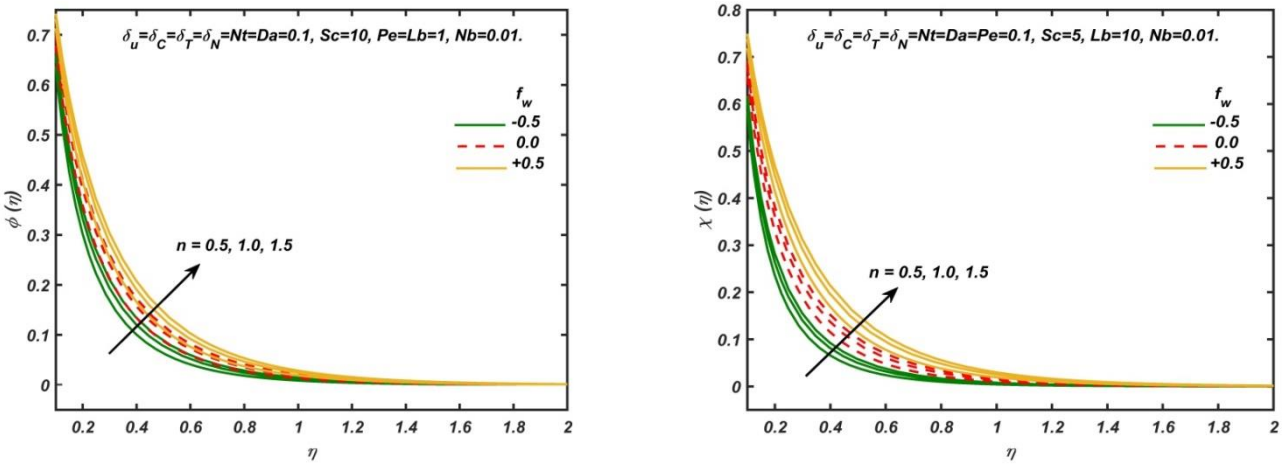

(a) **(b)**

Figure 3 Effect of blowing and power-law rheological index parameters on (a) the dimensionless nanoparticle concentration and (b) the microorganism density number.

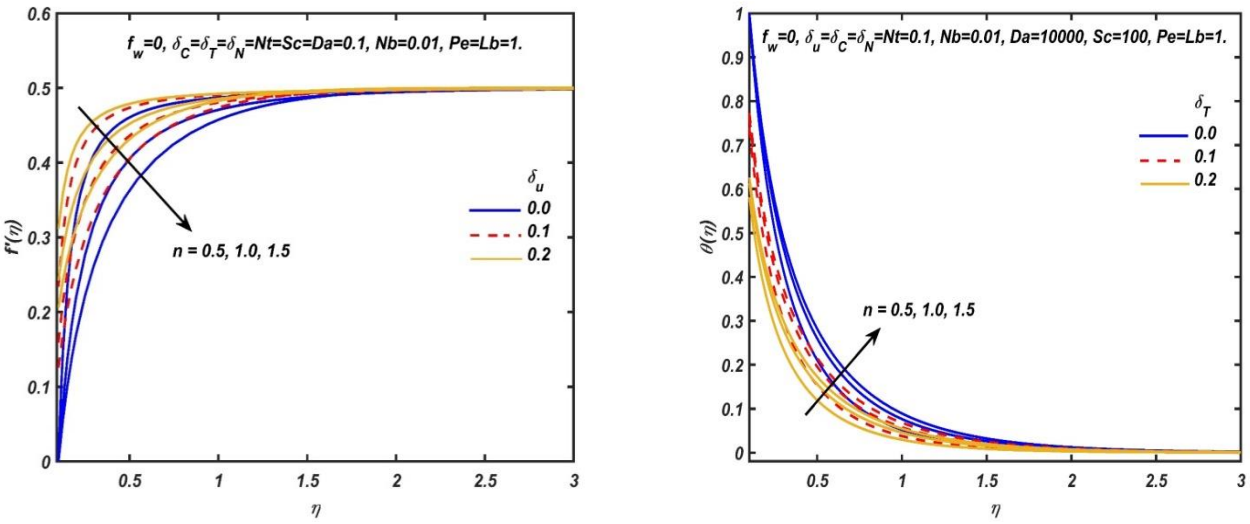

(a) **(b)**

Figure 4 Effect of (a) velocity slip on the dimensionless velocity and (b) thermal slip on the temperature.

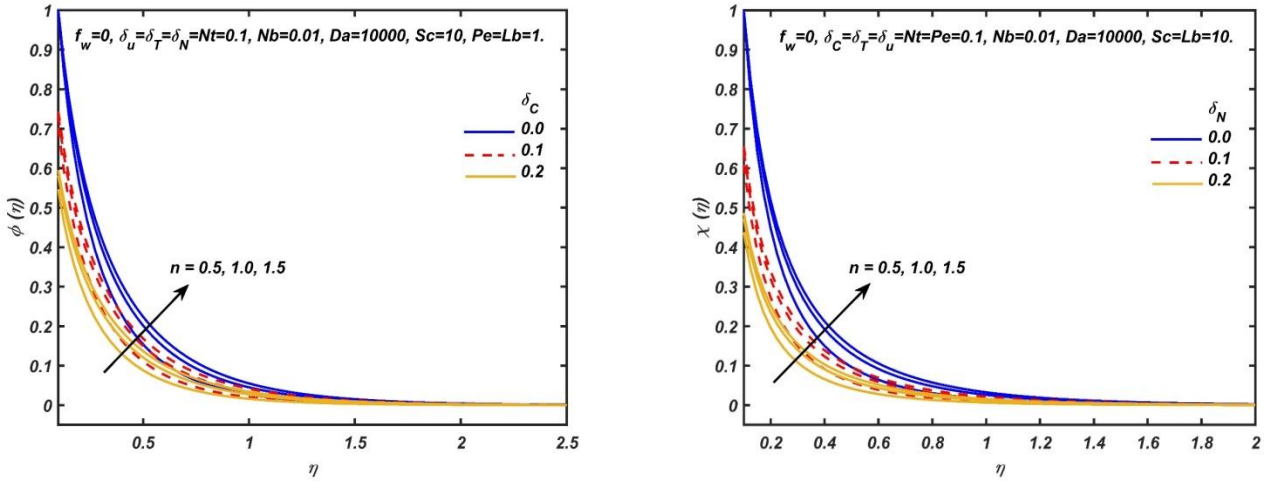

(a) **(b)**

Figure 5 Effect of (a) mass slip on the dimensionless concentration and (b) microorganism slip on the microorganism density number.

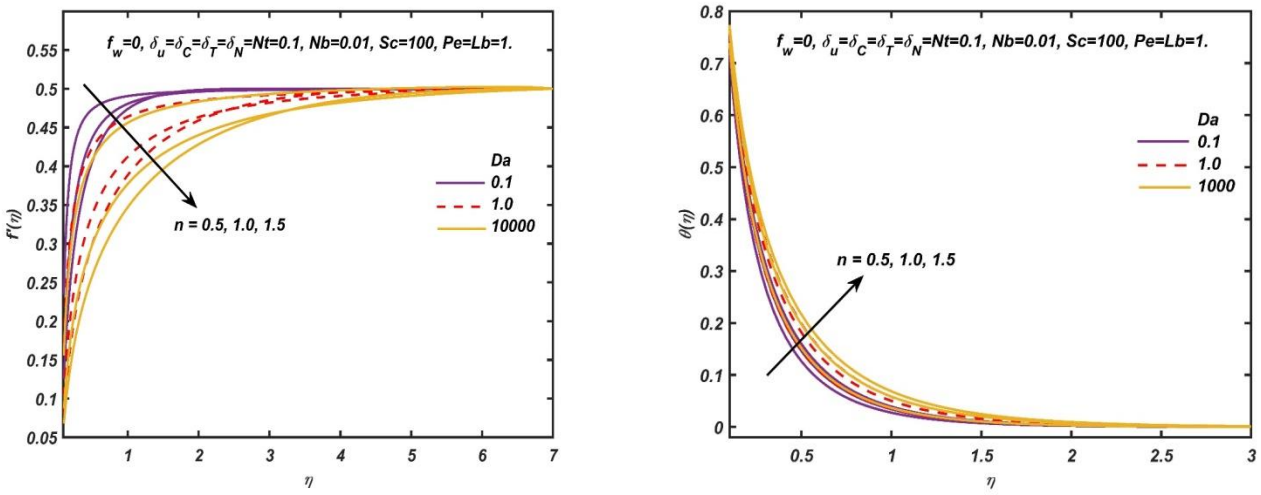

(a) **(b)**

Figure 6 Effect of Darcy number and power-law rheological index parameter on (a) the dimensionless velocity and (b) the dimensionless temperature.

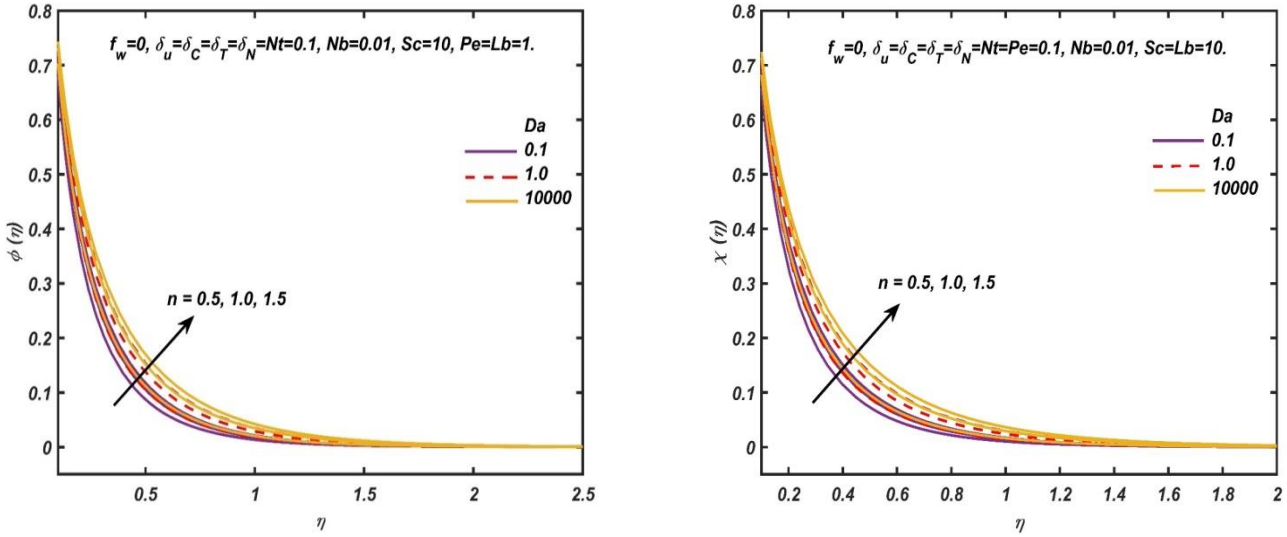

(a) **(b)**

Figure 7 Effect of Darcy number and power-law rheological index parameter on (a) the dimensionless concentration and (b) the dimensionless microorganism density number.

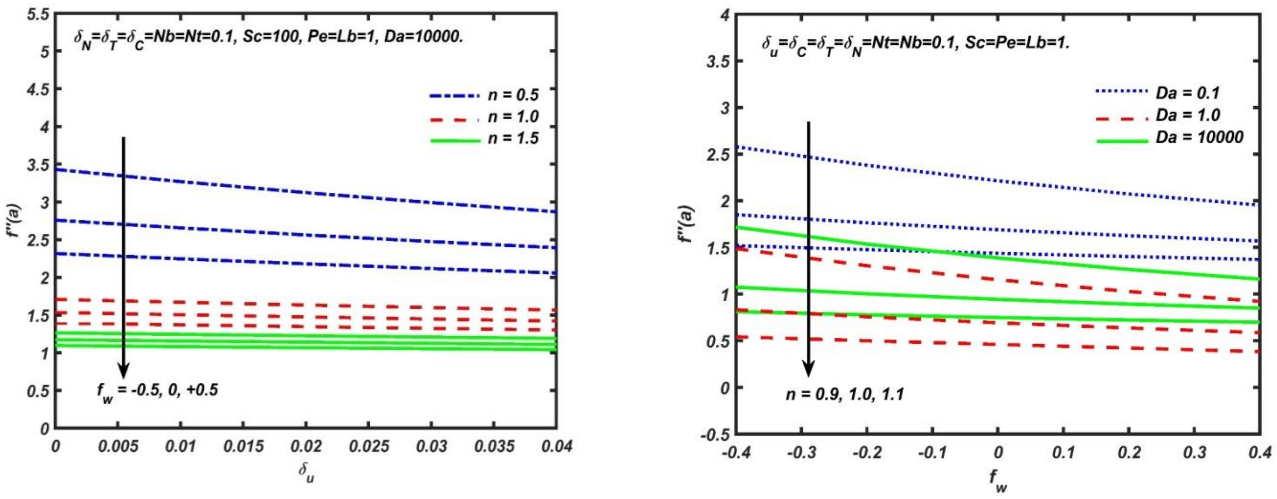

(a) **(b)**

Figure 8 Variations of skin friction with (a) the blowing, velocity slip, and power-law rheological index parameters and (b) the blowing, Darcy number, and power law rheological index parameters.

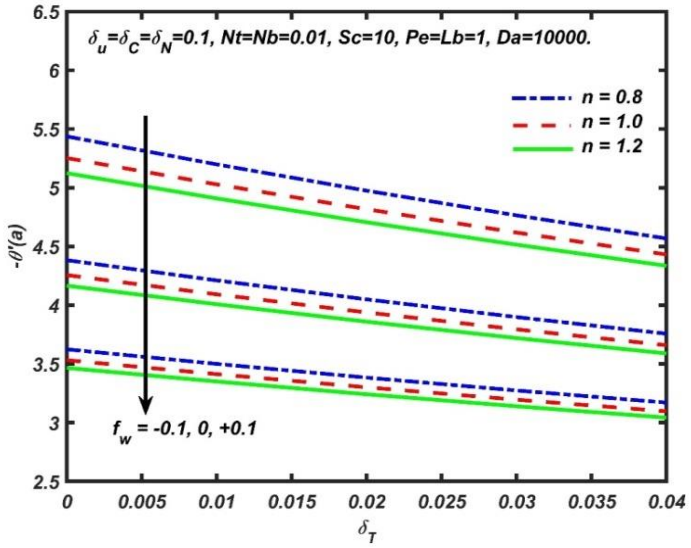

Figure 9 Variations of heat transfer rates with thermal slip, blowing, and power-law rheological index parameters.

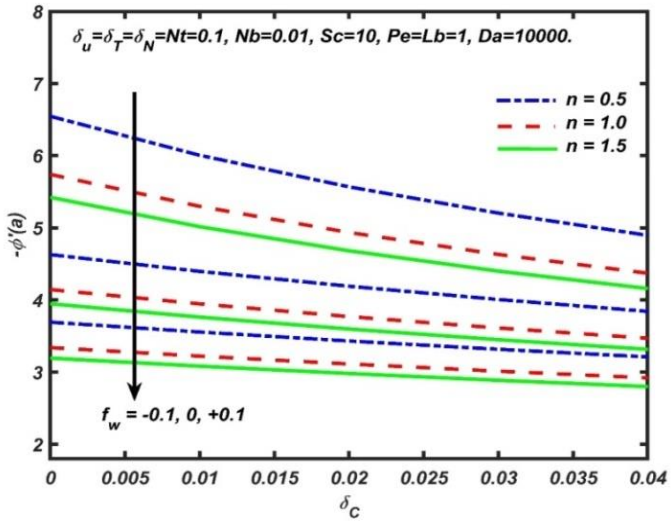

Figure 10 Variations of nanoparticle mass transfer rates with mass slip, blowing, and power-law rheological index parameters

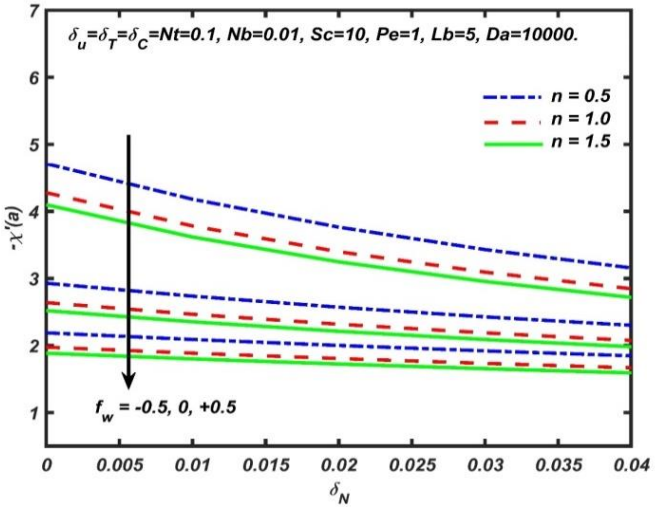

Figure 11 Variations of microorganism density number gradients with microorganism slip, blowing, and power-law rheological index parameters.

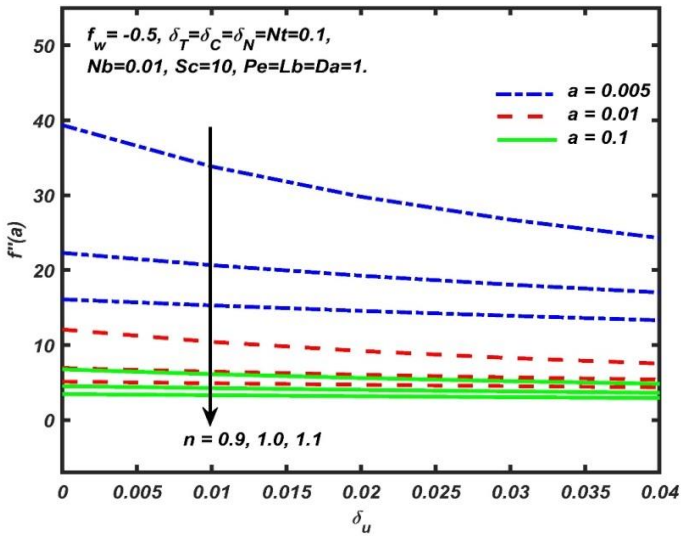

Figure 12 Variations of skin friction with velocity slip, needle size, and power-law rheological index parameters.

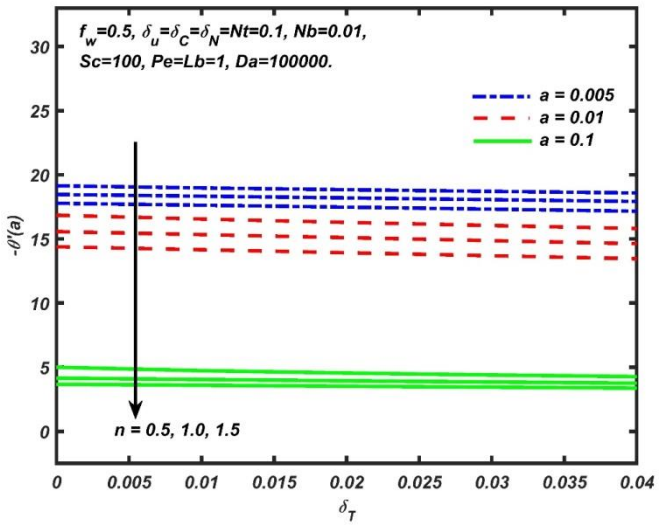

Figure 13 Variations of heat transfer rates with thermal slip, needle size, and power-law rheological index parameters.

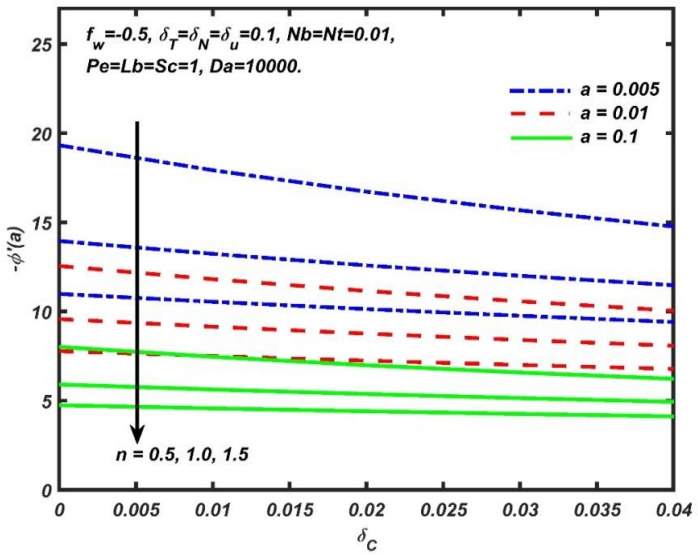

Figure 14 Variations of nanoparticle mass transfer rates with thermal slip, needle size, and power-law rheological index parameters.

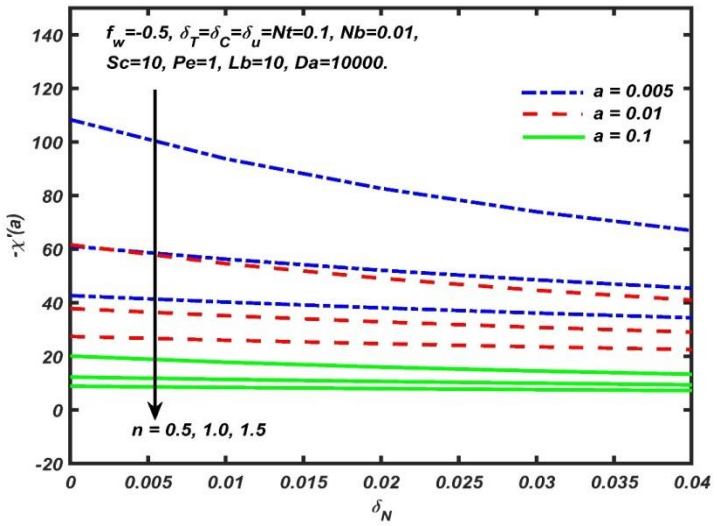

Figure 15 Variations of microorganism density number gradients with thermal slip, needle size, and power-law rheological index parameters.

The influence of the rheological power law parameter, *n*, and blowing parameter *fw* on the dimensionless velocity, temperature, nanoparticle concentration and motile microorganism density number, are shown in **Figs. 2 - 3**. From figure 2(a), it is clear that the velocity is considerably reduced with enhancing *n from 0.5 (pseudoplastic) to 1.5 (dilatant) for all three cases (i) the mass blowing (fw>0), (ii) no blowing (fw=0) i.e. solid needle surface, and (iii) suction (fw<0)*. In the case of $n < 1$ (e.g. 0.5), the non-Newtonian nanofluid displays *shear-thinning* properties and exhibits a reduced viscosity compared with conventional Newtonian fluids ($n = 1$). This leads to faster momentum diffusion rates, an escalation in the flow velocity and an associated reduction in momentum boundary layer thickness. On the contrary, in the case of $n > 1$ (e.g. 1.5), the fluid is *shear-thickening* and kinematic viscosity is boosted. This inhibits the momentum diffusion in the boundary layer and induces flow deceleration and a thicker momentum boundary layer on the needle. The Newtonian case naturally falls in between the shear thinning and shear thickening cases. The implication is that Newtonian models do not sufficiently predict the actual momentum characteristics, since these require for realistic needle coatings the inclusion of

rheological properties. With non-Newtonian effects, there is a significant deviation in the velocity characteristics from the classical Newtonian model ($n = 1$). The effects of n are also considerable in the vicinity of the wall (surface) of the needle ($\eta = a$). Excellent convergence of solutions is shown by the merging of all profiles to the far field value at $\eta = 3.5$ (approx.) It is further noteworthy that the thickness of the velocity (hydrodynamic) boundary layer for shear thinning nanofluids is lower than for Newtonian nanofluid, while the opposite case is apparent for shear thickening nanofluid. From figure 2(b), it is observed that a marked growth in temperature accompanies an increase in n from 0.5 through 1 to 1.5. Physically, with an increase of viscosity of the nanofluid, momentum diffusion is reduced, but since the Prandtl number is fixed, thermal diffusion is simultaneously increased. This leads to an elevation in thermal boundary layer thickness. Temperatures calculated for shear thickening (dilatant) nanofluids ($n > 1$) are clearly greater than those for shear thinning (pseudoplastic) nanofluids ($n < 1$). A rise in n (figure 3(a)) strongly enhances the nanoparticle concentration i.e., boosts the diffusion of nanoparticles which leads to a reduction the thickness of concentration boundary layer *for all three cases (i) the mass blowing (fw>0), (ii) no blowing (fw=0), and (iii) suction (fw<0).* This exacerbation in nanoparticle diffusion is again associated with the reduction in momentum diffusion with greater viscosity of the non-Newtonian nanofluid. A similar phenomenon is also apparent for the density number of micro-organisms (Fig. 3b). As the power-law index n increases, the temperature, the volume fraction, and motile micro-organism density number magnitudes all increase. Furthermore, with an increasing power-law index, the non-Newtonian nanofluid has a larger thermal, nanoparticle species and motile micro-organisms concentration boundary layer thicknesses. Moreover, increasing the power-law index leads to deceleration of the flow as blowing parameter changes from -0.5 (lateral mass influx) via 0 (solid needle) to 0.5 (lateral mass efflux) for all three types of nanofluids (pseudoplastic, Newtonian and dilatant).

Figures 4-5 (a, b) illustrate the effects of momentum slip (δ_u), thermal slip and nanoparticle species slip) (δ_T, δ_C) and microorganism slip (δ_N) respectively on transport characteristics. **Fig. 4(a)** depicts the simultaneous effects of the power-law parameter (*n*) and velocity slip parameter (δ_u) on the dimensionless velocity. It is found that a rise in δ_u leads to increase the dimensionless velocity near the wall $(\eta = a)$ of the needle for all three types of fluid. However greater velocities are computed for the pseudoplastic case as compared to either the Newtonian or dilatant case. The wall slip effect generally accelerates the flow, although the effect is confined largely to the boundary zone (at and near to the surface of the needle). Dimensionless temperature, concentration, and microorganism density number as plotted in Figures 4(b) & 5 (a, b), however *decrease* with an increase in δ_T, δ_C and δ_N respectively. As thermal slip parameter δ_T increases, the nanofluid in contact with the surface (wall) of the needle will not sense the heating effects of the needle and reduced heat will be released from the wall of the needle to the surrounding potential flow. A similar effect will be experienced via the nanoparticle and microorganism slip effects i.e. reduced species of either nanoparticles or micro-organisms will be released leading to a depletion in the magnitudes of both in the boundary layer regime.

Fig. 6 (a-b) demonstrates the collective effects of the power-law parameter (*n*) and Darcy number (*Da)* on the dimensionless velocity and temperature. The effect of Darcy number (defined by $Da = k_0 / \rho A_1 A_2$) on the dimensionless velocity is shown in Fig. 4(a). It is found that a rise in *Da* leads to a decrease in the dimensionless velocity near the wall of the needle for all three types of fluid. Temperature, concentration, and microorganism profiles in Figures 6(b) & 7 (a, b), however increased with the increase of Da . Physically, a rise of the Darcy number reduces the contribution of the term $-(1/Da)(2f'-1)$ (last term in the momentum Eqn. 11) and thus reduce the velocity. In the region close to the needle wall, the reduction of porous media drag results by a reduction in the presence of porous media fibers, i.e. an increase in *Da will decrease the flow.* This is contradicts

the behaviour usually encountered in porous media transport. The alteration in response is due to the *presence of pressure gradient*, which counteracts the usual accelerating effect accompanying an increase in Darcy number (increase in dimensionless permeability, *Da*) via the corresponding decrease in Darcian body force. With the increase of *Da*, temperatures (Fig. 6 (b)) are evidently increased within the thermal boundary layer region. Increasing permeability decreases the concentration of solid particles in the regime i. e. increases the presence of voids. The thermal conduction heat transfer is suppressed in the regime and this induces a cooling effect i.e. reduces temperatures.

We now consider the effects of various thermophysical parameters on the skin friction, the wall heat transfer rate (Nusselt number), nanoparticle wall mass transfer rate (Sherwood number) and motile microorganism density number gradient which are key engineering design parameters. **Figure 8(a)** depicts the variations of the skin friction with power-law rheological parameter, velocity slip and blowing parameters. It is found that skin friction reduces with an increment in the blowing parameter *from fw=-0.5 via 0 to 0.5* and power-law parameter, *both in the presence and absence* of momentum (velocity) slip. It is also found from figure 8(b) that skin friction decreases with an increase in Darcy number. The variations of the Nusselt number with power-law parameter, thermal slip, and blowing parameters are depicted in **Figure 9**. The results show that the heat transfer rates decrease with greater blowing, and power law parameters for both in the presence and absence of the thermal slip. This behaviour concurs with earlier studies on non-isothermal convection from a plate in uniform flow [54]. The variations of the Sherwood number with power law parameter, nanoparticle species slip and blowing parameters are illustrated in **Figure 10**. It is observed that nanoparticle mass transfer rates reduce with the increase of the blowing parameter and power law parameter, both when nanoparticle mass slip is absent or present. A similar trend is also noticed for motile microorganism density number gradient (Fig.11).

The MATLAB computations in this paper show that Nusselt number, nanoparticle species Sherwood number and microorganism density number gradient for power-law nanofluids are of significantly higher than for regular power-law fluids without microorganisms – see Gorla & Kumari [55] i.e. in the absence of bioconvection. Enhanced heat, mass and microorganism transfer rates are therefore accomplished for power-law fluids by *combining* both nanoparticles and microorganisms. This is helpful in increasing wall cooling in, for example bio-polymer material coating designs [56].

The modification in wall transport characteristics with needle size are shown in **Figures 12-15**. It is found that heat transfer rates (figure 13) are reduced with an increase in the needle size, both in the presence and absence of slip conditions and for all three types of fluids. Physically, this means that the consequence of needle transverse curvature is of significance - a more *slender needle* assists heat transfer, mass transfer and microorganism transfer rates, which is consistent with the modern trend for miniaturized hypodermic needle designs in nanomedicine. A similar trend of the heat transfer rates is also observed for regular fluid and for nanofluid flow [46]. Skin friction, nanoparticle mass transfer rate (Sherwood number) and microorganism density number gradient (Figs 14-15) are also found to be reduced with greater needle size, both in the presence and absence of slip conditions, for all three types of fluids (pseudoplastic, Newtonian and dilatant).

5.Conclusions

A new mathematical model for axisymmetric nanofluid forced bioconvection boundary layer flow of water-based non-Newtonian nanofluid over a solid thin needle located in Darcy porous medium (e.g. tissue) has been developed. Gyrotactic microorganisms are considered which do not interact with the spherical nanoparticles. To get physically realistic and practically applicable results, multiple slip boundary conditions and Stefan blowing at the wall have been incorporated in the model. The governing nonlinear partial differential conservation equations (NPDEs) have been

transformed into a set of similarity ordinary differential equations (SODEs) and then solved numerically using the in-built bvp4c function available in MATLAB software. Validation of the MATLAB solutions with the special case of Newtonian non-isothermal flow have been included. Careful selection of realistic nanofluid, thermophysical, geometric and bioconvection data has been conducted. The principal conclusions from the study can be summarized as follows:

- Velocity decreases whilst temperature, concentration and density number of motile microorganisms increase with an increment in blowing parameter for shear thinning, Newtonian and shear thickening nanofluids.
- Velocity increases with an increase in momentum slip whereas temperature, nanoparticle concentration and density number of motile microorganisms decrease with a rise in *thermal, mass and microorganism slip* for shear thinning fluid, Newtonian fluid, and shear thickening nanofluids.
- Skin friction decreases with elevation in blowing, Darcy and power law rheological parameters.
- Nusselt number, nanoparticle Sherwood number and motile microorganism density number gradient all decrease with a boost in the blowing, power-law, and needle size parameters.

In the current study a relatively simple non-Newtonian formulation has been adopted. Future investigations may include *viscoelastic* rheological models to simulate more accurately the elastic and viscous properties of coatings. Furthermore, for high velocity hypodermic needle injections in the subcutaneous tissue, non-Darcy effects may be investigated. The results of these studies will be reported imminently.

Acknowledgments

The authors are grateful to both reviewers for their comments which have helped to improve the present article.

References

[1] Nield, D. A. & Bejan, A. (2017). *Convection in Porous Media*. 5th ed. New York: Springer.

[2] Vafai, K. (2010). *Porous Media: Applications in Biological Systems and Biotechnology*. CRC

[3] Sachithanadam, M. & Joshi, S. C. (2016). *Silica Aerogel Composites*. 1st ed. Singapore: Springer

[4] Kasaeian, A., Daneshazarian, R., Mahian, O., Kolsi, L., Chamkha, A. J., Wongwises, S. & Pop, I. (2017). Nanofluid flow and heat transfer in porous media: a review of the latest developments. *International Journal of Heat and Mass Transfer* 107: 778-791.

[5] Cevc G, Vierl U. (2010). Nanotechnology and the transdermal route: a state-of-the-art review and critical appraisal. *J. Control. Release.* 141(3):277–99.

[6] E. Larrañeta *et al*., (2016). Microneedles: a new frontier in nanomedicine delivery, *Pharm Res.* 33: 1055–1073.

[7] Degim IT, Burgess DJ, Papadimitrakopoulos F. (2010). Carbon nanotubes for transdermal drug delivery. *J Microencapsul.* 27(8):669–81.

[8] Ferri, F. F. (2001). *Practical Guide to the Care of the Medical Patient*, 5th ed. St. Louis, MO: Mosby.

[9] Perry, J., and J. Jagger. *(*2002). Safer Needles: Not Optional. *Nursing* 32, 20-22.

[10] Ratzlaff, J. I. 2002. Needle safety technology. *Spinal Cord Injury Nursing* 19, 17-20.

[11] Ishak, A., Nazar, R. & Pop, I. (2007). Boundary layer flow over a continuously moving thin needle in a parallel free stream. *Journal of Chinese Physics Letters* 24(10): 2895-2897.

[12] Trimbitas, R., Grosan, T. & Pop, I.(2014). Mixed convection boundary layer flow along vertical thin needles in nanofluids. *International Journal of Numerical Methods for Heat and Fluid Flow* 24: 579–594

[13] Hayat, T., Khan, M. I., Farooq, M., Yasmeen, T. & Alsaedi, A. (2016). Water-carbon nanofluid flow with variable heat flux by a thin needle. *Journal of Molecular Liquids* 224: 786-791

[14]Bano, N. & Singh, B. B. (2017). An integral treatment for coupled heat and mass transfer by natural convection from a radiating vertical thin needle in a porous medium. *International Communications in Heat and Mass Transfer* 84: 41-48.

[15] Afridi, M. I. & Qasim, M. (2018). Entropy generation and heat transfer in boundary layer flow over a thin needle moving in a parallel stream in the presence of nonlinear Rosseland radiation. *International Journal of Thermal Sciences* 123: 117-128.

[16] Krishna, P. M., Sharma, R. P. & Sandeep, N. (2017). Boundary layer analysis of persistent moving horizontal needle in Blasius and Sakiadis magnetohydrodynamic radiative nanofluid flows. *Nuclear Engineering and Technology* 49(8): 1654-1659.

[17] Sulochana, C., Ashwinkumar, G. P. & Sandeep, N. (2017). Joule heating effect on a continuously moving thin needle in MHD Sakiadis flow with thermophoresis and Brownian moment. *The European Physical Journal Plus*, 132(9): 387.

[18] Afridi, M. I., Tlili, I., Qasim, M. & Khan, I. (2018). Nonlinear Rosseland thermal radiation and energy dissipation effects on entropy generation in CNTs suspended nanofluids flow over a thin needle. *Boundary Value Problems* 2018(1): 1-14.

[19] Salleh, S. N. A., Bachok, N., Arifin, N. M., Ali, F. M. & Pop, I. (2018). Magnetohydrodynamics flow past a moving vertical thin needle in a nanofluid with stability analysis. *Energies* 11(12): 297.

[20] Souayeh, B., Reddy, M. G., Sreenivasulu, P., Poornima, T., Rahimi-Gorji, M. & Alarifi, I. M. (2019). Comparative analysis on non-linear radiative heat transfer on MHD Casson nanofluid past a thin needle. *Journal of Molecular Liquids* 284: 163-174.

[21] Minkowycz, W. J., Sparrow, E., & Abraham, J. P. (2013). *Nanoparticle Heat Transfer and Fluid Flow*. New York: Taylor and Francis Group, CRC press.

[22] Shenoy, A. V. (1994). Non-Newtonian fluid heat transfer in porous media. In *Advances in Heat transfer* 24: 101-190.

[23] Myers, T. G., Ribera, H. & Cregan, V. (2017). Does mathematics contribute to the nanofluid debate? *International Journal of Heat and Mass Transfer* 111: 279-288.

[24] Etaig, S., Hasan, R. & Perera, N. (2018). A new effective viscosity model for nanofluids. *International Journal of Numerical Methods for Heat and Fluid Flow* 28(3): 571-583.

[25] Mahian, O., Kolsi, L., Amani, M., Estellé, P., Ahmadi, G., Kleinstreuer, C., Marshall, J. S., Siavashi, M., Taylor, R. A., Niazmand, H., Hayat, T., Kolanjiyil, A., Kasaeian, A., Pop, I. & Wongwises, S. (2019). Recent Advances in Modelling and Simulation of Nanofluid Flows-Part II: applications. *Physics Reports* 791: 1-59.

[26] Bold, H. C. & Wynne, M. J. (1978). *Introduction to the Algae: Structure and Reproduction, Prentice-Hall, Englewood Cliffs*. USA: New Jersey.

[27] Mil-Martínez, R., Ferrer, V. H., Turcio, M., López-Serrano, F., Ortega, J. A. & Vargas, R. O.(2019). Stability analysis and numerical simulation of gravitactic bioconvection in a rectangular cavity. *Computers and Mathematics with Applications* 77(1): 222-236.

[28] Belabid, J. & Allali, K. (2019). Thermo-bioconvection in horizontal porous annulus with the presence of phototactic microorganisms. *International Journal of Engineering Science* 140: 17-25.

[29] Zohra, F. T., Uddin, M. J., Ismail, A. I. M., **Bég, O. Anwar** & Kadir, A. (2018). Anisotropic slip magneto-bioconvection flow from a rotating cone to a nanofluid with Stefan blowing effects. *Chinese Journal of Physics* 56(1): 432-448.

[30] Amirsom, N. A., Uddin, M. J. & Ismail, A. I. M. (2019). MHD boundary layer bio-nano-convective non-Newtonian flow past a needle with Stefan blowing. *Heat Transfer—Asian Research* 48(2): 727-743.

[31] **Bég, O. Anwar** (2018). Nonlinear multi-physical laminar nanofluid bioconvection flows: Models and computation. *A. Sohail, Z. Li (Eds.): Computational Approaches in Biomedical Nano-Engineering, Wiley-CVH, China.*

[32] Siddiqa, S., Sulaiman, M., Hossain, M. A., Islam, S. & Gorla, R. S. R. (2016). Gyrotactic bioconvection flow of a nanofluid past a vertical wavy surface. *International Journal of Thermal Sciences* 108: 244-250.

[33] Ferdows, M., A. Alsenafi, **O. Anwar Bég**, Tasveer A. Bég and Ali Kadir. (2021). Numerical study of nano-biofilm stagnation flow from a nonlinear stretching/shrinking surface with variable nanofluid and bio-convection transport properties, *Scientific Reports*, 11:9877 (21 pages).

[34] **Bég, O. Anwar**, Noman Kabir, Uddin M.J, Ahmad Izani Md. Ismail, Yasser Alginahi (2020). Numerical investigation of Von Karman swirling bioconvective nanofluid transport from a rotating disk in a porous medium with Stefan blowing and anisotropic slip effects, *Proc. IMechE-Part C- J. Mechanical Engineering Science*. DOI: 10.1177/ 0954406220973061 (19 pages.

[35] Zaman, S. & Gul, M. (2019). Magnetohydrodynamic bioconvective flow of Williamson nanofluid containing gyrotactic microorganisms subjected to thermal radiation and Newtonian conditions. *Journal of theoretical biology* 479: 22-28.

[36] Sochi, T. (2010). Non-Newtonian flow in porous media. *Polymer* 51(22): 5007-5023.

[37] Khan, W. A., Uddin, M. J. & Ismail, A. I. M. (2015). Bioconvective non-Newtonian nanofluid transport over a vertical plate in a porous medium containing microorganism in a moving free stream. *Journal of Porous Media* 18(4): 389-399.

[38] Kefayati, G. H. R. (2016). Heat transfer and entropy generation of natural convection on non-Newtonian nanofluids in a porous cavity. *Powder Technology* 299: 127-149.

[39] Huang, C. J. (2018). Influence of non-Darcy and MHD on free convection of non-Newtonian fluids over a vertical permeable plate in a porous medium with Soret/Dufour effects and thermal radiation. *International Journal of Thermal Sciences* 130: 256-263.

[40 Waqas, H., Khan, S. U., Hassan, M., Bhatti, M. M. & Imran, M. (2019). Analysis on the bioconvection flow of modified second-grade nanofluid containing gyrotactic microorganisms and nanoparticles. *Journal of Molecular Liquids* 291: 111231.

[41] Amirsom, N. A., Uddin, Basir, M. F., Kadir, A., **Bég, O. Anwar** & Izani, A. (2019). Computation of melting dissipative magnetohydrodynamic nanofluid bioconvection with second-order slip and variable thermophysical properties. *Applied Sciences* 9(12): 2493.

[42] Roy, A.K., **O. Anwar Bég**, Apu Kumar Saha and J. V. Ramana Murthy (2021), Taylor dispersion in non-Darcy porous media with bulk chemical reaction: a model for drug transport in impeded blood vessels, *J. Engineering Mathematics*, 127:24 (18 pages) (2021).

[43] Umavathi, J.C. and **O. Anwar Bég**. (2021). Simulation of the onset of convection in porous medium layer saturated by a couple stress nanofluid, *Microfluidics and Nanofluidics. 25: 53 https://doi.org/10.1007/s10404-021-02448-5 (20 pages).*

[44] Rehman, Aysha, Azad Hussain, and Sohail Nadeem. Assisting and opposing stagnation point pseudoplastic nano liquid flow towards a flexible Riga sheet: a computational approach. *Mathematical Problems in Engineering* 2021 (2021).

[45] Rizwana, Rizwana, Azad Hussain, and Sohail Nadeem. Mixed convection non-boundary layer flow of unsteady MHD oblique stagnation point flow of nanofluid. *International Communications in Heat and Mass Transfer* 124 (2021): 105285.

[46] Ahmad, S., Nadeem, S. and Khan, M.N., 2021. Mixed convection hybridized micropolar nanofluid with triple stratification and Cattaneo–Christov heat flux model. *Physica Scripta*, *96*(7), p.075205.

[47] Hussain, Azad, Aysha Rehman, Sohail Nadeem, M. Y. Malik, Alibek Issakhov, Lubna Sarwar, and Shafiq Hussain. A combined convection carreau–yasuda nanofluid model over a convective heated surface near a stagnation point: a numerical study. *Mathematical Problems in Engineering* 2021 (2021).

[48] Hossen, Md Belal, Harun-Or Roshid, and Md Zulfikar Ali. Modified Double Sub-equation Method for Finding Complexiton Solutions to the (1+ 1) Dimensional Nonlinear Evolution Equations. *International Journal of Applied and Computational Mathematics* 3, no. 1 (2017): 679-697.

[49] Or-Roshid, Harun, and M. M. Rashidi. Multi-soliton fusion phenomenon of Burgers equation and fission, fusion phenomenon of Sharma–Tasso–Olver equation. *Journal of Ocean Engineering and Science* 2, no. 2 (2017): 120-126.

[50] Schlichting, H. & Gersten, K. (2017). *Boundary-Layer Theory*. 9th ed. Berlin: Springer.

[51] Lienhard IV, J. H. & Lienhard, J. H. (2005). *A Heat Transfer Textbook*. 3rd ed. (662–663) Cambridge USA: Phlogiston Press.

[52] Chen, J. L. S. & Kearns Jr, J. W. (1983). Forced convection in non-Newtonian flow past a non-isothermal needle. *ASME Journal of Heat Transfer* 105(4): 919-922.

[53] Hairer, E., Lubich, C. & Wanner, G. (2006). *Geometric numerical integration: structure-preserving algorithms for ordinary differential equations.* 2nd ed. Berlin: Springer.

[54] Uddin, M. J., Yusoff, N. M., **Bég, O. Anwar** & Ismail, A. I. (2013). Lie group analysis and numerical solutions for non-Newtonian nanofluid flow in a porous medium with internal heat generation. *Physica Scripta*, 87(2): 025401.

[55] Gorla, R. & Kumari, M. (2003). Free convection in non-Newtonian fluids along a horizontal plate in a porous medium. *Heat and Mass Transfer* 39(2): 101-106.

[56] Raykar, V. S. & Singh, A. K. (2010). Thermal and rheological behavior of acetylacetone stabilized ZnO nanofluids. *Thermochimica Acta* 502(1-2): 60-65.